

# A model of tear-film breakup with continuous mucin concentration and viscosity profiles

Mohar Dey<sup>1</sup>, Atul S. Vivek<sup>2</sup>, Harish N. Dixit<sup>2</sup>, Ashutosh Richhariya<sup>3</sup>  
and James J. Feng<sup>1,4,†</sup>

<sup>1</sup>Department of Mathematics, University of British Columbia, Vancouver, BC V6T 1Z2, Canada

<sup>2</sup>Department of Mechanical and Aerospace Engineering, Indian Institute of Technology Hyderabad,  
Kandi, Sangareddy 502285, India

<sup>3</sup>L. V. Prasad Eye Institute, Hyderabad, Telangana 500034, India

<sup>4</sup>Department of Chemical and Biological Engineering, University of British Columbia,  
Vancouver, BC V6T 1Z3, Canada

(Received 30 April 2018; revised 20 September 2018; accepted 22 September 2018)

We propose an alternative to the prevailing framework for modelling tear-film breakup, which posits a layered structure with a mucus layer next to the cornea and an aqueous layer on top. Experimental evidence shows continuous variation of mucin concentration throughout the tear film, with no distinct boundary between the two layers. Thus, we consider a continuous-viscosity model that replaces the mucus and aqueous layers by a single liquid layer with continuous profiles of mucin concentration and viscosity, which are governed by advection–diffusion of mucin. The lipids coating the tear film are treated as insoluble surfactants as previously, and slip is allowed on the ocular surface. Using the thin-film approximation, we carry out linear stability analysis and nonlinear numerical simulations of tear-film breakup driven by van der Waals attraction. Results show that for the same average viscosity, having more viscous material near the ocular surface stabilizes the film and prolongs the breakup time. Compared with the layered models, the continuous-viscosity model predicts film breakup times that are in better agreement with experimental data. Finally, we also suggest a hydrodynamic explanation for how pathological loss of membrane-associated mucins may lead to faster breakup.

**Key words:** interfacial flows (free surface), thin films

---

## 1. Introduction

The tear film contains a mixture of various proteins and other biomolecules secreted by the basal epithelial cells and the surrounding meibomian and lacrimal glands. The stability of this thin protective film is essential to the health of the eye as it shields the ocular surface from harmful environmental factors and pathogens (Selinger, Selinger, & Reed 1979; Mantelli & Argueso 2008; Stevenson, Chauhan & Dana 2012; Yañez-Soto *et al.* 2014). Traditionally, the tear film is visualized as comprising

† Email address for correspondence: [james.feng@ubc.ca](mailto:james.feng@ubc.ca)

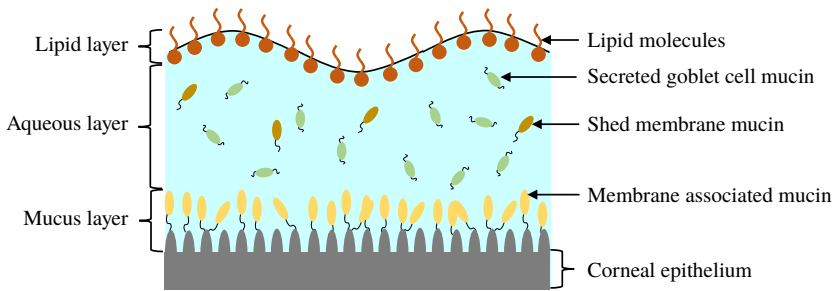


FIGURE 1. (Colour online) Schematic illustration of the composition and structure of the pre-corneal tear film.

three distinct layers (Braun 2012), as schematically shown in figure 1. The innermost mucus layer, 0.2–0.5  $\mu\text{m}$  in thickness, is composed of membrane-associated mucins (MAMs) that form the glycocalyx on the corneal epithelium (Gipson 2004), and serves as a barrier that protects the cornea from pathogens. The mucins also maintain hydration and wettability of the ocular surface (Hodges & Dartt 2013). Outside the mucus layer lies the aqueous layer (2.5–5  $\mu\text{m}$ ) that forms the bulk of the tear film. It consists primarily of aqueous tear fluid produced by the lacrimal glands with some gel-forming mucins secreted by the conjunctival goblet cells (Inatomi *et al.* 1996). Finally, lipids secreted from the meibomian glands form a monolayer (0.02–0.05  $\mu\text{m}$ ) atop the aqueous layer, which helps stabilize the air–tear interface and reduce evaporation (Craig & Tomlinson 1997; McCulley & Shine 1997; Bron *et al.* 2004).

Our understanding of the hydrodynamics of the tear film has been summarized in a comprehensive review by Braun (2012). A focus of interest is the breakup process, which may occur through several different mechanisms (King-Smith, Begley & Braun 2018). One is an instability driven by van der Waals attraction (Sharma & Ruckenstein 1985, 1986*a,b*; De Wit, Gallez & Christov 1994; Craster & Matar 2009). Another is due to evaporation (Liu *et al.* 2009; Peng *et al.* 2014; Siddique & Braun 2015; Braun *et al.* 2018). Finally, tear films can also rupture very rapidly owing to non-uniformities in the lipid layer (Siddique & Braun 2015; Zhong *et al.* 2018). Our work focuses on the first mechanism due to van der Waals attraction. As explained in the following, our primary goal is to reconcile previous van der Waals-based models with a more realistic description of the tear-film structure.

Most of our understanding of this mode of tear-film rupture has come from single-layer models (Zhang, Craster & Matar 2003*b*; Braun & King-Smith 2007; Heryudono *et al.* 2007; Winter, Anderson & Braun 2010; Deng, Braun & Driscoll 2014; Siddique & Braun 2015) and two-layer models (TLMs) (Sharma & Ruckenstein 1985, 1986*a,b*; Zhang, Craster & Matar 2003*a*, 2004). The former overlook the structure of the tear film and assign a uniform viscosity throughout its thickness. The latter posit an interface separating the aqueous and mucus layers, with its own interfacial tension as well as van der Waals interactions with the other surfaces. Most of these models assume a flat ocular surface and initially flat fluid interfaces, given the small thickness of the tear film relative to the radius of curvature ( $\sim 1$  cm) of the corneal globe (Braun 2012). In the same vein, the thin-film or lubrication approximation is always adopted even though the interface may take on sharp curvatures towards the instant of rupture (Oron, Davis & Bankoff 1997). The

main findings of these models are that the tear film ruptures as the result of an instability driven by van der Waals attraction (De Wit *et al.* 1994; Craster & Matar 2009), and that the instability is resisted to some extent by the interfacial tension as well as a Marangoni stress that arises from the lipids on the tear film that act as insoluble surfactants (Berger & Corrsin 1974; Zhang *et al.* 2003*b*). Some studies have considered slip on the ocular surface (Zhang *et al.* 2003*b*; Braun & King-Smith 2007; Heryudono *et al.* 2007), and found that slip facilitates the instability and promotes tear-film rupture. This scenario reflects the outcome of an infection in the mucus layer that may compromise the glycocalyx to induce slip on the substrate. Even though the human tear is known to be shear-thinning (Tiffany 1991), non-Newtonian rheology has only been considered in a few studies (Zhang *et al.* 2003*a*, 2004; Jossic *et al.* 2009; Braun *et al.* 2012).

As noted by Braun (2012), more recent experiments have challenged the picture of the layered tear film. Mucin is found throughout the tear film (Prydal & Campbell 1992; Chen *et al.* 1997; Bron *et al.* 2004; Gipson 2004; Govindarajan & Gipson 2010). In the absence of a distinct boundary between the aqueous and the mucus layers, the mucin concentration forms a continuous profile within the entire tear film. To better reflect the structure of the tear film, we propose a continuous-viscosity model (CVM) as an alternative to the prevailing uniform single-layer models and TLMs. Drawing from analysis of miscible two-fluid flows in a different context (Ern, Charru & Luchini 2003; Usha, Tammisola & Govindarajan 2013; Ghosh, Usha & Sahu 2014), we introduce advection–diffusion for the mucin throughout a single, continuous tear film, which modifies the viscosity profile and in turn the hydrodynamics of the breakup.

Compared with existing models, the CVM enjoys several advantages. First, it avoids the difficulty of determining the properties of the putative mucin–aqueous interface, including the interfacial tension and van der Waals interactions (Sharma & Ruckenstein 1986*a*; Zhang *et al.* 2003*a*). Moreover, by varying the mucin diffusivity, one can model healthy tear films in which an immobile membrane-tethered mucin population maintains a permanent mucin gradient, as well as pathological conditions where mucin detachment and diffusion modify the viscosity profile and, in turn, the breakup process. Thus, the model can provide a potential linkage between the hydrodynamic features of the breakup and the onset and progression of eye infection. Finally, the model can be generalized to account for additional mechanisms in tear-film dynamics. For example, one can explicitly model the growth and proliferation of bacterial colonies in a similar fashion to mucin. Although at present we only consider viscosity as a function of the mucin concentration, viscoelasticity of the polymers can be introduced straightforwardly.

The rest of this paper is organized as follows. In § 2, we present the CVM for the tear film, with details of non-dimensionalization and parameter values. Then we present the linear stability analysis in § 3 and the nonlinear simulations in § 4. In § 5, we compare our model predictions with those of the TLM and with experimental data. Conclusions are drawn in § 6.

## 2. Mathematical formulation

### 2.1. Problem description

We model the entire tear film as a mucin solution in a Newtonian solvent, with an initial mucin concentration profile  $C_0(y)$ . The lipids on the free surface are treated as insoluble surfactants that advect and diffuse on the interface, with a surface tension  $\sigma$

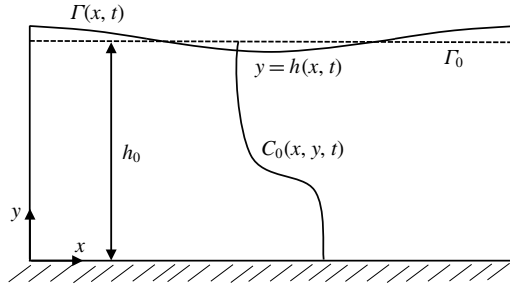


FIGURE 2. Schematic representation of the computational domain of a tear film with the CVM.

that depends on the local surfactant concentration  $\Gamma$ . We assume isothermal conditions and neglect evaporation from the free surface and loss of fluid or mucins due to osmosis from the ocular surface (Siddique & Braun 2015). The tear film rests on top of a rough impermeable substrate, the corneal epithelium, on which we impose the Navier slip condition with slip length  $\beta$ . Starting from the initial profile  $C_0(y)$ , the mucin concentration  $C(x, y, t)$  evolves according to an advection–diffusion equation. The viscosity  $\mu(x, y, t)$  is an algebraic function of  $C(x, y, t)$ , and thus its profile evolves accordingly. The tear film has constant density  $\rho$ .

On the two-dimensional domain of figure 2 we pose the incompressible Navier–Stokes equations governing the flow dynamics together with an advection–diffusion equation describing the mucin redistribution:

$$\nabla \cdot \mathbf{u} = 0, \tag{2.1}$$

$$\rho \left( \frac{\partial \mathbf{u}}{\partial t} + \mathbf{u} \cdot \nabla \mathbf{u} \right) = -\nabla(p + \phi) + \nabla \cdot \boldsymbol{\tau}, \tag{2.2}$$

$$\frac{\partial C}{\partial t} + \mathbf{u} \cdot \nabla C = D_b \nabla^2 C, \tag{2.3}$$

where  $\mathbf{u} = (u, v)$  is the velocity vector and  $D_b$  is the bulk diffusivity for the mucin transport. Here  $p$  is pressure and  $\phi = -\mathcal{A}/(6\pi h^3)$  is the disjoining pressure due to van der Waals attraction, with  $\mathcal{A}$  being the unretarded Hamaker constant (Ruckenstein & Jain 1974; William & Davis 1982). The deviatoric stress tensor is given by

$$\boldsymbol{\tau} = \mu(y) \begin{bmatrix} 2\frac{\partial u}{\partial x} & \frac{\partial u}{\partial y} + \frac{\partial v}{\partial x} \\ \frac{\partial u}{\partial y} + \frac{\partial v}{\partial x} & 2\frac{\partial v}{\partial y} \end{bmatrix}. \tag{2.4}$$

The surface of the tear film  $y = h(x, t)$  evolves according to the kinematic condition (Oron *et al.* 1997):

$$\frac{\partial h}{\partial t} + \frac{\partial}{\partial x} \left( \int_0^{h(x,t)} u \, dy \right) = 0. \tag{2.5}$$

On the surface, the lipid concentration  $\Gamma(x, t)$  is governed by the following surfactant transport equation (Zhang *et al.* 2003a):

$$\frac{\partial \Gamma}{\partial t} + \nabla_s \cdot (\Gamma \mathbf{u}_s) + \Gamma (\nabla_s \cdot \mathbf{n})(\mathbf{u} \cdot \mathbf{n}) = D_s \nabla_s^2 \Gamma, \tag{2.6}$$

Parameter	Description	Value and source
$L$	Characteristic length	$5 \times 10^{-4}$ m (Braun <i>et al.</i> 2018)
$H$	Characteristic thickness	$3.5 \times 10^{-6}$ m (Braun <i>et al.</i> 2018)
$\beta$	Slip coefficient	$3.5 \times 10^{-7}$ m (Zhang <i>et al.</i> 2003b)
$\rho$	Density of tear film	$1.3 \times 10^3$ kg m <sup>-3</sup> (Deng <i>et al.</i> 2014)
$\mu_c$	Characteristic viscosity of tear film	$1.3 \times 10^{-3}$ Pa s (Tiffany 1991)
$\sigma_m$	Maximal interfacial tension	$4.5 \times 10^{-2}$ N m <sup>-1</sup> (Nagyová & Tiffany 1999)
$S$	Maximal spreading pressure	$7.5 \times 10^{-8}$ N m <sup>-1</sup> (Zhang <i>et al.</i> 2003a)
$\Gamma_m$	Maximal surfactant concentration	$4 \times 10^{-7}$ mol m <sup>-2</sup> (Bruna & Breward 2014)
$\mathcal{A}$	Unretarded Hamaker constant	$3.5 \times 10^{-19}$ Pa m <sup>3</sup> (Winter <i>et al.</i> 2010)
$D_s$	Surface diffusivity	$3 \times 10^{-8}$ m <sup>2</sup> s <sup>-1</sup> (Bruna & Breward 2014)
$D_b$	Bulk diffusivity	$4.5 \times 10^{-12}$ m <sup>2</sup> s <sup>-1</sup> (Gribbon & Hardingham 1998)

TABLE 1. Parameters in the model, along with the references used for estimating their values.

where  $\mathbf{n}$  is the normal vector on the surface,  $\nabla_s = (\mathbf{I} - \mathbf{nn}) \cdot \nabla$  is the surface divergence operator,  $\mathbf{u}_s = \mathbf{u} - \mathbf{nn} \cdot \mathbf{u}$  is the tangential velocity vector and  $D_s$  is the surface diffusivity for the insoluble surfactant. Following Zhang *et al.* (2003a), we assume that  $\Gamma$  is dilute and the interfacial tension  $\sigma$  decreases linearly with  $\Gamma$ :  $\sigma(\Gamma) = \sigma_m - S\Gamma/\Gamma_m$ , where  $\sigma_m$  is the maximal interfacial tension on a lipid-free interface,  $S$  is the maximal spreading pressure and  $\Gamma_m$  is the maximum lipid concentration. We have the normal and tangential stress balances at  $y = h(x, t)$ :

$$\mathbf{n} \cdot \boldsymbol{\tau} \cdot \mathbf{n} = p - \sigma(\nabla \cdot \mathbf{n}), \quad (2.7)$$

$$\mathbf{n} \cdot \boldsymbol{\tau} \cdot \mathbf{t} = \nabla \sigma \cdot \mathbf{t}. \quad (2.8)$$

On the solid substrate  $y = 0$ , we impose the Navier slip boundary condition with a slip length  $\beta$ :

$$u = \beta \frac{\partial u}{\partial y}, \quad v = 0. \quad (2.9a,b)$$

For the mucin transport, a no-flux boundary condition is imposed on the top and bottom of the domain,

$$\frac{\partial C}{\partial y} = 0. \quad (2.10)$$

On the left and right ends of the domain, we impose zero-slope conditions as in previous studies (Zhang *et al.* 2003b). The parameters of the model are summarized in table 1.

Our treatment of the mucin (and hence viscosity) profile requires some explanation. In healthy tear films, the glycocalyx consists of MAMs that form a more or less immobile polymer-rich layer. Meanwhile, soluble mucins produced at the conjunctiva diffuse freely in the tear film. The onset of ocular diseases often compromises the glycocalyx, forcing the MAMs to shed their ectodomains into the aqueous medium (Albertsmeyer *et al.* 2010; Govindarajan & Gipson 2010). The shed ectodomains then diffuse alongside the soluble mucins to elevate the bulk viscosity of the tear film. Our model does not represent the glycocalyx as a physical entity, and thus cannot

capture its structural remodelling directly or distinguish between the membrane-bound and soluble species of mucins. Instead, we represent the healthy and diseased states of the mucin profile through the diffusivity  $D_b$ . For the diseased state, where all mucins diffuse in the bulk of the tear film, we adopt the  $D_b$  value for biopolymers having similar molecular weights to the mucins (Gribbon & Hardingham 1998; Celli *et al.* 2005), direct measurement of mucin diffusivity being unavailable in the literature. This value, listed in table 1, marks the upper bound of  $D_b$  as all mucins diffuse freely in this case, with a diffusion time scale of a second. Lower  $D_b$  values will be used to maintain large gradients of mucin during the course of tear-film breakup. The healthy tear film will be represented by a much lower  $D_b$  that produces a nearly permanent glycocalyx with little diffusion. Admittedly simplistic, this is an easy way to reflect the changing mucin profiles without modelling the kinetics of structural changes.

## 2.2. Non-dimensionalization

The above system of equations and boundary conditions are non-dimensionalized using the following scaling:

$$\left. \begin{aligned} x^* &= \frac{x}{L}, & y^* &= \frac{y}{H}, & h^* &= \frac{h}{H}, & \beta^* &= \frac{\beta}{H}, \\ u^* &= \frac{u}{V}, & v^* &= \frac{Lv}{HV}, & t^* &= \frac{tV}{L}, & p^* &= \frac{p}{P}, \\ \Gamma^* &= \frac{\Gamma}{\Gamma_m}, & \sigma^* &= \frac{\sigma}{\sigma_m}, \end{aligned} \right\} \quad (2.11)$$

where

$$V = \frac{A}{6\pi\mu_c HL}, \quad P = \frac{A}{6\pi H^3} \quad (2.12a,b)$$

are the characteristic velocity and pressure, respectively. In the literature, the characteristic viscosity  $\mu_c$  is often taken to be that of ‘the aqueous layer’ (Zhang *et al.* 2003a). In our CVM context, we define it as the viscosity at the top of the tear film. Here  $H$  and  $L$  are the characteristic thickness and horizontal length scale respectively of an undisturbed tear film. Following Braun *et al.* (2018), we define  $L$  from a balance between viscous and capillary forces; it is much smaller than the physical dimension of the ocular surface.

Dimensionless equations are obtained on applying the above scaling to (2.1)–(2.6). For simplicity, we use the same symbols after the scaling, and all expressions below are dimensionless unless otherwise stated:

$$u_x + v_y = 0, \quad (2.13)$$

$$\epsilon^2 Re(u_t + uu_x + vv_y) = -(p + \phi)_x + 2\epsilon^2 \mu u_{xx} + [\mu(u_y + \epsilon^2 v_x)]_y, \quad (2.14)$$

$$\epsilon^4 Re(v_t + uv_x + vv_y) = -p_y + \epsilon^2 [\mu(u_y + \epsilon^2 v_x)]_x + 2\epsilon^2 (\mu v_y)_y, \quad (2.15)$$

$$C_t + uC_x + vC_y = \frac{1}{Pe_b} \left( C_{xx} + \frac{1}{\epsilon^2} C_{yy} \right), \quad (2.16)$$

where subscripts  $t$ ,  $x$  and  $y$  indicate partial derivatives with respect to that variable,  $\epsilon = H/L$  is the aspect ratio of the tear film,  $Re = \rho VL/\mu_c$  is the Reynolds number and  $Pe_b = VL/D_b$  is the Péclet number for bulk mucin diffusion. The boundary conditions

are  $u = \beta u_y$ ,  $v = 0$  and  $C_y = 0$  at  $y = 0$  (substrate), and the following at the free surface  $y = h(x, t)$ :

$$h_t + \left( \int_0^{h(x,t)} u \, dy \right)_x = 0, \tag{2.17}$$

$$\Gamma_t + \nabla_s \cdot (\Gamma \mathbf{u}_s) + \Gamma (\nabla_s \cdot \mathbf{n})(\mathbf{u} \cdot \mathbf{n}) = \frac{1}{Pe_s} \nabla_s^2 \Gamma, \tag{2.18}$$

$$p(1 + \epsilon^2 h_x^2) = \frac{2\epsilon^2 \mu}{1 + \epsilon^2 h_x^2} [\epsilon^2 u_x h_x^2 + v_y - (u_y + \epsilon^2 v_x) h_x] - \frac{Ch_{xx}}{(1 + \epsilon^2 h_x^2)^{1/2}}, \tag{2.19}$$

$$\mu[(1 - \epsilon^2 h_x^2)(u_y + \epsilon^2 v_x) - 4\epsilon^2 h_x u_x] = -\frac{\epsilon Ma \Gamma_x}{Ca} (1 + \epsilon^2 h_x^2)^{1/2}, \tag{2.20}$$

$$C_y = 0, \tag{2.21}$$

where  $Pe_s = VL/D_s$  is the surface Péclet number for the surfactant diffusion,  $Ma = (\Gamma_m/\sigma_m)(\partial\sigma/\partial\Gamma)$  is the Marangoni number,  $Ca = \mu_c V/\sigma_m$  is the capillary number and  $C = \epsilon^3/Ca$  (Sharma & Ruckenstein 1986a,b; Oron *et al.* 1997).

### 2.3. Thin-film approximation

Since the tear film is very thin relative to its transverse dimension, with an aspect ratio  $\epsilon \ll 1$ , we can neglect the inertial and the higher-order  $\epsilon$  terms. Thus, using the lubrication approximation (Oron *et al.* 1997), we obtain the following set of equations at the leading order in  $\epsilon$ :

$$u_x + v_y = 0, \tag{2.22}$$

$$-p_x - \phi_x + (\mu u_y)_y = 0, \tag{2.23}$$

$$p_y = 0, \tag{2.24}$$

$$C_t + uC_x + vC_y = C_{yy}/\Delta_b, \tag{2.25}$$

where  $\Delta_b = \epsilon^2 Pe_b$  is the rescaled bulk Péclet number. As explained by Oron *et al.* (1997),  $\Delta_b$  can be  $O(1)$  despite the appearance of  $\epsilon^2$ , in the limit of very large  $Pe_b$  or very small  $D_b$ , which is relevant to the case at hand. Thus, the  $\Delta_b$  term is retained to account for the mucin diffusion in the  $y$  direction. The above equations are subject to the following boundary conditions.

At  $y = 0$ ,

$$u = \beta u_y, \quad v = 0, \quad C_y = 0. \tag{2.26a-c}$$

At  $y = h(x, t)$ ,

$$h_t + \left( \int_0^{h(x,t)} u \, dy \right)_x = 0, \tag{2.27}$$

$$\Gamma_t + (u_s \Gamma)_x = \frac{\Gamma_{xx}}{Pe_s}, \tag{2.28}$$

$$p = -Ch_{xx}, \tag{2.29}$$

$$\mu u_y = -\mathcal{M} \Gamma_x, \tag{2.30}$$

$$C_y = 0, \tag{2.31}$$

where  $\mathcal{M} = \epsilon Ma/Ca$  is the rescaled ratio of Marangoni to capillary number, and it reflects the surfactant effects on the evolution of the free surface. Both the linear stability analysis and nonlinear simulations discussed in the following are based on the above set of equations after the lubrication approximation has been applied.

### 3. Linear stability analysis

We first carry out a linear stability analysis of (2.22)–(2.31). Initially the tear film is flat and stationary, with a height  $h_0 = 1$  and a uniform surfactant concentration  $\Gamma_0$ . Small perturbations are added to the initial state in the following form:

$$u = \tilde{u}(y)e^{ikx+\omega t}, \quad (3.1)$$

$$v = \tilde{v}(y)e^{ikx+\omega t}, \quad (3.2)$$

$$h = h_0 + \tilde{h}e^{ikx+\omega t}, \quad (3.3)$$

$$\Gamma = \Gamma_0 + \tilde{\Gamma}e^{ikx+\omega t}, \quad (3.4)$$

$$C = C_0(y) + \tilde{C}(y)e^{ikx+\omega t}. \quad (3.5)$$

The tilde quantities are assumed to be much smaller than the base-state variables, e.g.  $|\tilde{h}| \ll h_0$ . The initial concentration profile  $C_0(y)$  is arbitrary. This allows us to analyse the effect of an arbitrary initial viscosity profile  $\mu_0(y)$  on the stability of the thin film. Since we restrict ourselves to a two-dimensional analysis, it is convenient to define a stream function

$$\psi = \tilde{\psi}(y)e^{ikx+\omega t}, \quad (3.6)$$

such that  $u = \partial\psi/\partial y$  and  $v = -\partial\psi/\partial x$ . Substituting the above into the governing equations and retaining terms that are linear in the perturbations, we reduce the system to ordinary differential equations (ODEs) for  $\tilde{\psi}$  and  $\tilde{C}$ ,

$$(\mu_0\tilde{\psi}_{yy})_{yy} = 0, \quad (3.7)$$

$$\omega\tilde{C} + \frac{k^2\tilde{C}}{Pe_b} - \frac{\tilde{C}_{yy}}{\epsilon^2 Pe_b} = ik\tilde{\psi}, \quad (3.8)$$

with the following boundary conditions:

$$\mu_0\tilde{\psi}_{yy} + \mu_0\tilde{\psi}_{yyy} = -\frac{k^2}{\omega} \left( \frac{3}{h_0^4} - Ck^2 \right) \tilde{\psi}, \quad \mu\tilde{\psi}_{yy} = -\frac{k^2\mathcal{M}\Gamma_0}{\left(\omega + \frac{k^2}{Pe_s}\right)} \tilde{\psi}_y, \quad \tilde{C}_y = 0 \quad \text{at } y = h_0, \quad (3.9a-c)$$

$$\tilde{\psi} = 0, \quad \tilde{\psi}_y = \beta\tilde{\psi}_{yy}, \quad \tilde{C}_y = 0 \quad \text{at } y = 0. \quad (3.10a-c)$$

Equations (3.7)–(3.10) form an eigenvalue problem for  $\omega$ , and its real part determines the linear stability of the thin film. Note that as a consequence of zero mean flow in the film, the stream function  $\tilde{\psi}$  is decoupled from the concentration  $\tilde{C}$ . Thus, the linear stability of the film can be solved from (3.7) along with the boundary conditions; it will depend only on the initial viscosity profile. Then (3.8) and its boundary conditions can be solved for the evolution of the concentration and viscosity profiles.

Equations (3.7)–(3.10) admit analytical solutions for uniform, linear and Heaviside viscosity profiles. For an arbitrary viscosity profile, we employ a Chebyshev collocation technique to solve the eigenvalue problem numerically. If the viscosity profile contains a thin layer of steep gradient, as occurs across the diffuse outer boundary of the mucin layer, we use a coordinate transformation to ‘stretch out’ the layer for adequate resolution at moderate numerical cost. The accuracy of the numerical procedure is established by comparing the numerical solutions to analytical ones for two simple viscosity profiles. For a uniform viscosity profile, our numerical solution agrees closely with the analytical solution of Zhang *et al.* (2003b) (figure 3a).

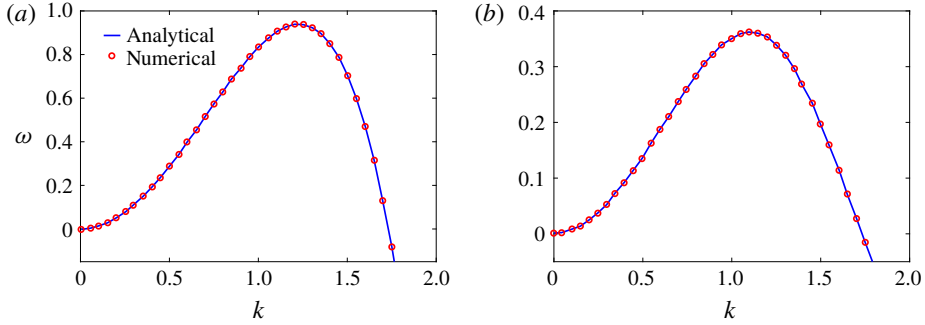


FIGURE 3. (Colour online) Comparisons between numerically computed dispersion relations and analytical solutions. (a) For a uniform viscosity profile  $\mu_0 = 1$  with surface Péclet number  $Pe_s = 0.1$ . The analytical solution is from Zhang *et al.* (2003b). (b) For a tanh viscosity profile with a sharp transition layer, with parameters  $\delta_m = 0.01$ ,  $h_m = 0.2$ ,  $\mu_r = 2$  and  $Pe_s = 100$ . The analytic solution is from the TLM of Zhang *et al.* (2003a). The other parameters are  $h_0 = 1$ ,  $\Gamma_0 = 0.5$ ,  $C = 1$ ,  $\mathcal{M} = 1$  and  $\beta = 0.1$ .

To approximate a two-layer setup with a sharp jump in viscosity, we use a tanh profile with a thin transition layer of thickness  $\delta_m$  at a height of  $y = h_m$ :

$$\mu_0(y) = 1 + \frac{\mu_r - 1}{2} \left( 1 - \tanh \frac{y - h_m}{\delta_m} \right), \quad (3.11)$$

where  $\mu_0$  is scaled by the viscosity at the top of the aqueous layer and  $\mu_r$  is the viscosity ratio between the bottom and the top of the tear film. Similar viscosity profiles were used in recent studies on stability of viscosity-stratified free-surface flows down an incline (Usha *et al.* 2013). On the other hand, we take the analytical solution of a TLM (Zhang *et al.* 2003a) and put to zero the interfacial tension between the two layers as well as the van der Waals attractions between the liquid interface and both the top and the bottom boundaries ( $C_m = 0$ ,  $\mathcal{A}_{1,2,4} = 0$  as defined in appendix A). Thus, the TLM and the continuous tanh model approach a common limit, and the dispersion relations are again in excellent agreement in this limit (figure 3b). These tests validate the numerical procedure for solving the eigenvalue problem.

### 3.1. Effect of the viscosity profile

We examine the linear instability of four different viscosity profiles with the same average viscosity: a uniform profile, two linear profiles with opposite slopes and a tanh profile (figure 4a). To compare the growth rate  $\omega$  among the four profiles, we need to adjust its scaling somewhat. Our general scheme of non-dimensionalization (2.12) uses the viscosity  $\mu_c$  at the top of the tear film to define a time scale. Here the four viscosity profiles share the same average viscosity but not the same  $\mu_c$ . To scale  $\omega$  uniformly, we have made an exception to the general scheme by adopting, for all four cases, the time scale based on the top viscosity of the tanh profile. In such a scheme, the common average viscosity  $\mu_a = 1.5$  for all four profiles (figure 4a).

Figure 4(b) shows that the viscosity distribution has a marked effect on the growth rate of the instability. If the more viscous fluid is situated at the bottom of the film, the growth rate is lower and the film is relatively more stable. Between the two profiles with negative gradients (i.e.  $\partial\mu_0/\partial y < 0$ ), the tanh profile has lower growth

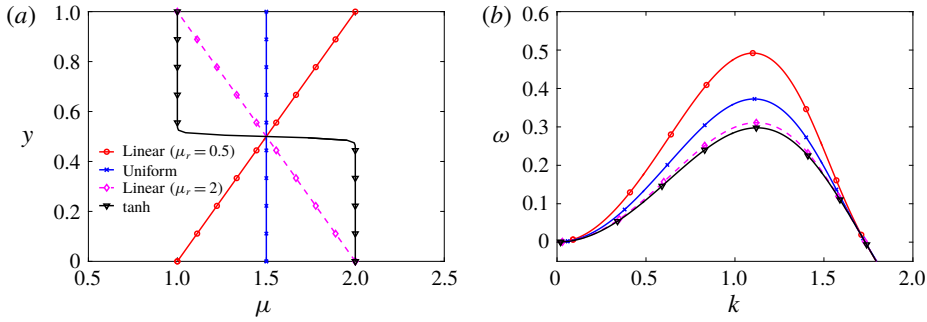


FIGURE 4. (Colour online) (a) Four different initial viscosity profiles, each with a mean dimensionless viscosity of 1.5. For the tanh viscosity profile,  $\mu_r = 2$ ,  $h_m = 0.5$  and  $\delta_m = 0.01$ . (b) Dispersion relations for the four viscosity profiles. The parameter values are  $h_0 = 1$ ,  $\Gamma_0 = 0.5$ ,  $\mathcal{C} = 1$ ,  $\mathcal{M} = 1$ ,  $\beta = 0.1$  and  $Pe_s = 100$ .

rate as it has more high-viscosity fluid in the bottom half of the film. To understand this stabilization by more viscous fluids near the substrate, we investigate the linear viscosity profile further, as it allows an analytical solution.

### 3.2. Analytical solution for linear viscosity profiles

We parametrize the linear viscosity in terms of  $\mu_r$ , the viscosity ratio between the bottom ( $y = 0$ ) and the top ( $y = 1$ ) of the film:

$$\mu_0(y) = \mu_r - (\mu_r - 1)y. \tag{3.12}$$

Inserting the above into (3.7), we integrate with respect to  $y$  four times to obtain

$$\tilde{\psi} = \frac{c_1 y^2}{2(\mu_r - 1)} - \frac{\mu_r c_1 + (\mu_r - 1)c_2}{(\mu_r - 1)^3} (\mu_0 \ln \mu_0 - \mu_0) + c_3 y + c_4, \tag{3.13}$$

where  $c_1, \dots, c_4$  are constants of integration to be determined from the four boundary conditions in (3.9)–(3.10). The algebra of determining the eigenvalue  $\omega$  is simplified if we neglect Marangoni flow ( $\mathcal{M} = 0$ ) and slip on the bottom wall ( $\beta = 0$ ). Under these conditions, the growth rate  $\omega$  can be expressed as

$$\omega = k^2 (3 - Ck^2) \left[ \frac{1}{2(\mu_r - 1)} - \frac{1}{(\mu_r - 1)^2} + \frac{\ln \mu_r}{(\mu_r - 1)^3} \right], \tag{3.14}$$

where  $k$  is the wavelength.

In order to compare the growth rate for linear viscosity profiles having the same average viscosity but different slopes, it is convenient to parametrize the dimensional viscosity profile using the average viscosity  $\mu_a$  and the slope  $\mu_s$ :  $\mu_0(y) = \mu_a + \mu_s(y - h_0/2)$ . Then the growth rate can be scaled uniformly using the time scale based on  $\mu_a$ . In the limit of gentle slope, with  $|\mu_s h_0 / \mu_a| \ll 1$ , equation (3.14) can be recast into the following form for the rescaled growth rate:

$$\tilde{\omega} = k^2 (3 - Ck^2) \left[ \frac{1}{3} + \frac{1}{12} \frac{\mu_s h_0}{\mu_a} + O\left(\frac{\mu_s^2 h_0^2}{\mu_a^2}\right) \right]. \tag{3.15}$$

If the region of higher viscosity is located near  $y = 0$ ,  $\mu_s < 0$  and the growth rate is reduced relative to a uniform viscosity profile of the same mean viscosity. This explains the trend observed in figure 4(b).

#### 4. Nonlinear numerical simulation

In the linear analysis, the equations governing the flow field and mucin transport (3.7) and (3.8) are decoupled and, as a result, the consequences of mucin diffusion cannot be studied within the linear framework. We therefore resort to a numerical solution of the nonlinear lubrication equations (2.22)–(2.31). Because the mucin diffusion equation is solved in two dimensions, our problem cannot be reduced to a set of one-dimensional partial differential equations as in earlier nonlinear studies of thin-film flows (Zhang *et al.* 2003a,b; Pototsky *et al.* 2004).

##### 4.1. Problem setup and numerics

The mucin concentration field evolves in the two-dimensional domain whose upper boundary, the surface of the film, changes in time. To avoid solving a moving boundary system in the domain  $x \in [0, L]$ ,  $y \in [0, h(x, t)]$ , we introduce a mapping

$$\eta = \frac{y}{h(x, t)} \quad (4.1)$$

that transforms the tear film into a rectangular domain  $x \in [0, L]$ ;  $\eta \in [0, 1]$ . Accordingly, the governing equations are transformed into the  $(x, \eta)$  coordinates:

$$u_x - u_\eta \frac{\eta}{h} h_x + \frac{v_\eta}{h} = 0, \quad (4.2)$$

$$-(p + \phi)_x + \frac{1}{h^2} (\mu u_\eta)_\eta = 0, \quad (4.3)$$

$$C_t - C_\eta \frac{\eta}{h} h_t + u \left( C_x - C_\eta \frac{\eta}{h} h_x \right) + v \frac{C_\eta}{h} = \frac{1}{\Delta_b} \frac{C_{\eta\eta}}{h^2}, \quad (4.4)$$

subject to the following boundary conditions. At  $\eta = 1$ ,

$$h_t + u h_x = v, \quad (4.5)$$

$$\Gamma_t + (u\Gamma)_x = \frac{\Gamma_{xx}}{Pe_s}, \quad (4.6)$$

$$\mu \frac{u_\eta}{h} = -\mathcal{M}\Gamma_x, \quad (4.7)$$

$$p = -\mathcal{C}h_{xx}, \quad (4.8)$$

$$C_\eta = 0, \quad (4.9)$$

and at  $\eta = 0$ ,

$$u = \beta \frac{u_\eta}{h}, \quad v = 0, \quad C_\eta = 0. \quad (4.10a-c)$$

After solving the problem in the  $(x, \eta)$  plane, the solution is transformed back to the  $(x, y)$  plane for visualization and analysis.

We impose the following sinusoidal initial perturbation:

$$h(x, 0) = h_0 + \tilde{h}e^{ik_m x}, \quad (4.11)$$

$$\Gamma(x, 0) = \Gamma_0 + \tilde{\Gamma}e^{ik_m x}, \quad (4.12)$$

$$C(x, y, 0) = C_0(y) + \tilde{C}e^{ik_m x}, \quad (4.13)$$

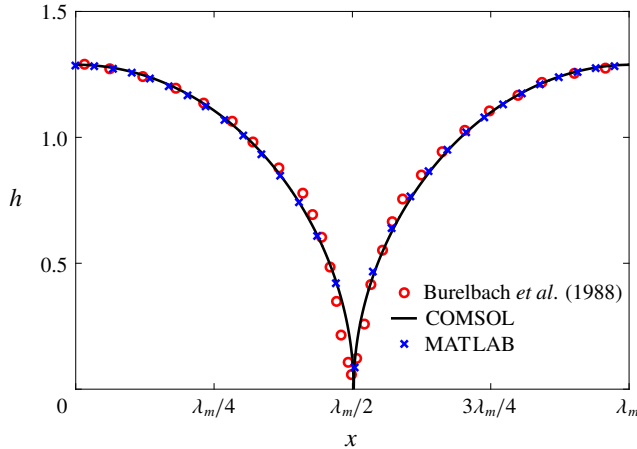


FIGURE 5. (Colour online) Validation of our numerical schemes: the instantaneous interfacial profile of a liquid film at the moment of rupture, computed using two different methods and compared with the result of Burelbach, Bankoff & Davis (1988). The abscissa is labelled in terms of the fastest-growing wavelength  $\lambda_m$ .

where  $k_m$  is the wavenumber of the fastest growing mode of linear instability, and the small initial amplitudes  $(\tilde{h}, \tilde{\Gamma}, \tilde{C})$  are calculated by solving the set of equations (3.7)–(3.10) with  $\tilde{h} = 0.01$ . The dimensionless initial conditions have  $h_0 = 1$  and  $\Gamma_0 = 0.5$ . The initial mucin concentration profile is

$$C_0(y) = 1 + \frac{\mu_r - 1}{2} \left( 1 - \tanh \frac{y - h_m}{\delta_m} \right), \quad (4.14)$$

and we adopt a dimensionless viscosity

$$\mu(C) = C, \quad (4.15)$$

ignoring the solvent contribution relative to the mucin contribution. In addition, a linear and uniform profile will also be tested in § 4.4 for comparison, as has been done in the linear stability analysis of § 3.

To solve the nonlinear film breakup problem outlined above, we have used two independent numerical methods. One is the finite-element solver COMSOL 5.2, and the other is an in-house MATLAB solver that uses a central difference scheme in the  $x$  direction and a Chebyshev pseudo-spectral discretization in the  $\eta$  direction, along with an Adam–Moulton time-stepping scheme. As validation, we have computed the one-dimensional problem of an isothermal film breakup, with constant viscosity and no surfactant, for which a solution is available in the literature (Burelbach *et al.* 1988). To be consistent with Burelbach *et al.* (1988), we impose periodic boundary conditions between the left and right edges of the domain. For the parameter set of figure 4 of Burelbach *et al.* (1988), figure 5 shows that our two numerical procedures produce essentially identical results, agreeing closely with the earlier result of Burelbach *et al.* (1988). In particular, we have predicted rupture times  $t_{rup} = 4.085$  using COMSOL and  $t_{rup} = 4.072$  using the MATLAB solver, close to  $t_{rup} = 4.164$  predicted by Burelbach *et al.* (1988). In the following, we will only present results computed using COMSOL, as all cases computed using our MATLAB solver yielded essentially the same results.

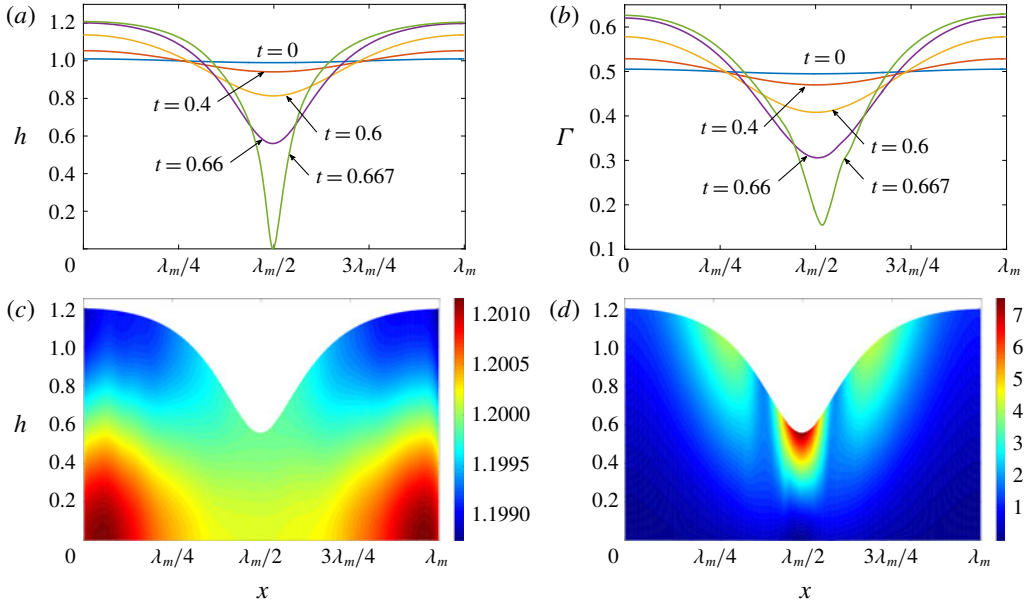


FIGURE 6. (Colour online) A representative solution of nonlinear film breakup. (a) Temporal evolution of the interface and (b) evolution of the surfactant concentration until rupture at  $t = 0.667$ . (c) Contours of the mucin concentration and (d) contours of the magnitude of the velocity in the tear film at  $t = 0.66$ , just before rupture.

#### 4.2. General characteristics of film rupture

Figure 6 presents a representative solution for the evolution of the interface to rupture, using the following baseline set of parameters:  $h_m = 0.2$ ,  $\mu_r = 2$ ,  $\delta_m = 10^{-2}$ ,  $\mathcal{C} = 0.1$ ,  $\mathcal{M} = 1$ ,  $Pe_s = 100$ ,  $\Delta_b = 1$  and  $\beta = 0.1$ . Starting from the small disturbance imposed on the surface of a uniform stationary film (4.11)–(4.13), a pressure gradient due to the short-range van der Waals forces causes the disturbance to grow (figure 6a) by moving liquid from the valley to the crest region. This flow also transports the insoluble surfactant on the surface (figure 6b), generating a Marangoni flow that tends to oppose the film thinning due to van der Waals force. Meanwhile, the mucin distribution deviates from its initial profile (4.14) by convection and diffusion (figure 6c). Although the Marangoni flow slows down film thinning to some extent, it is unable to overcome the destabilizing effect of the van der Waals attraction, and the thinning flow continues (figure 6d) until the film ruptures at  $t_{rup} = 0.667$ .

In the following, the film breakup is quantified in terms of the evolution of the free interface and the rupture time  $t_{rup}$ . We will compare the nonlinear instability with the predictions of linear growth, and analyse how film rupture is affected by the mucin diffusivity and the initial mucin concentration profile. Unless otherwise stated, we will vary the parameters relative to the baseline values given above. We have also explored the effects of slip on the ocular surface and the magnitude of the van der Waals forces. These turn out to be qualitatively the same as reported earlier for a single-layer model (Zhang *et al.* 2003b) and TLMs (Sharma & Ruckenstein 1986a,b; Zhang *et al.* 2003a). As expected, larger slip and stronger van der Waals attraction both lead to faster growth and breakup. We omit these results for brevity.

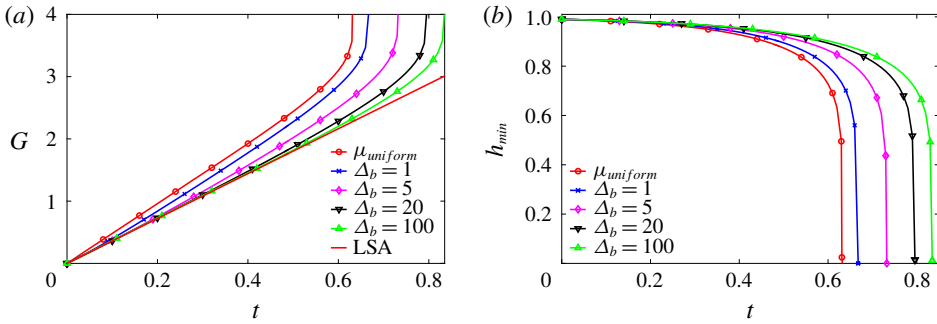


FIGURE 7. (Colour online) Nonlinear growth of the instability as affected by mucin diffusivity,  $\Delta_b$  being the rescaled Péclet number. (a) Comparison of the nonlinear growth metric  $G$  with the linear growth (LSA). (b) Temporal evolution of the minimum height  $h_{min}$  for the nonlinear cases. For comparison, we have included in both plots the solution for a uniform-viscosity film whose viscosity equals the average viscosity of the tanh profile.

#### 4.3. Effect of mucin diffusivity

In the nonlinear phase of the instability, the higher order terms are no longer negligible and mucin diffusion plays a key role. Following Matar (2002), we define a nonlinear growth metric

$$G = \ln \left[ \frac{h_{max}(t) - h_{min}(t)}{h_{max}(0) - h_{min}(0)} \right], \quad (4.16)$$

where  $h_{max}(t)$  and  $h_{min}(t)$  are the maximum and minimum film thickness at time  $t$ , and compare it to the linear growth  $\omega_m t$ ,  $\omega_m$  being the fastest growth rate among the linear modes of instability.

Using the tanh initial mucin profile with the baseline parameters, we have tested several values of the rescaled Péclet number  $\Delta_b$  for mucin diffusion (2.25), and compared the nonlinear growth against the linear prediction in figure 7(a). Note first that the nonlinear curves coincide with the linear result at short times, as is expected. Later the growth rate increasingly deviates from the prediction of linear instability, resulting in a catastrophic rupture at the end (figure 7b), as opposed to the exponential rupture predicted by linear instability. Among the four nonlinear growth curves, the rupture occurs faster for the smaller values of  $\Delta_b$ , i.e. larger mucin diffusivity. This can be rationalized from our linear analysis of the effect of the viscosity profile. Figure 4 shows that having high-viscosity fluid near the solid boundary tends to suppress the linear growth rate and stabilize the film. In the nonlinear regime, the mucin diffuses from the near-wall region, where  $C$  is the highest, towards the free surface of the film, where  $C$  is the lowest. This dynamically lowers the viscosity near the substrate and raises it near the free surface, thereby accelerating the instability according to the linear analysis. Thus, higher mucin diffusivity leads to faster growth and earlier rupture.

It is interesting to examine the limits of rapid and slow diffusion. As discussed in § 2, the rapid diffusion at the  $D_b$  value of table 1 ( $\Delta_b = 4.4 \times 10^{-4}$ ) corresponds to complete loss of the MAMs and free diffusion of mobile mucins. Diffusion being so rapid, the tear film behaves essentially as if with a uniform initial viscosity profile, shown by the curve labelled by  $\mu_{uniform}$  in figure 7. At the slow diffusion limit,

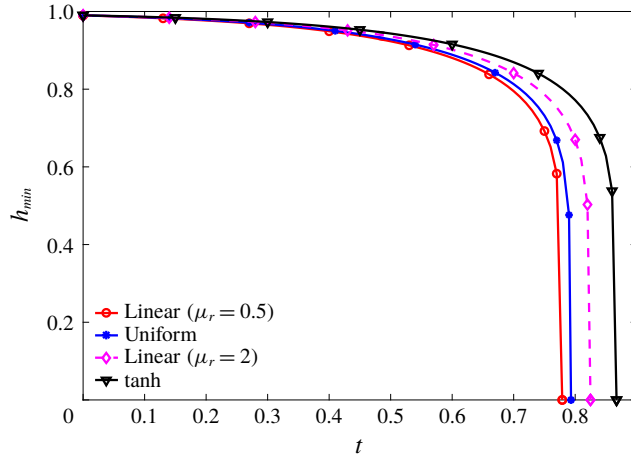


FIGURE 8. (Colour online) Evolution of the minimum film thickness  $h_{min}(t)$  for the four initial viscosity profiles of figure 4(a). Similar to figure 4(b), we have scaled time by the same characteristic time, corresponding to the tanh profile, for all four viscosity profiles.

represented by the curve for  $\Delta_b = 100$ , the mucin profile diffuses little during the breakup process, approximating the intact glycocalyx in a healthy tear film. In both limits, the tear film dynamics is insensitive to  $\Delta_b$ , and we have chosen an intermediate  $\Delta_b = 1$  as our baseline for the purpose of demonstrating the effect of mucin diffusion. We compare the model predictions of breakup time with experimental measurements on healthy tear films in § 5.3.

The transition from the slow to the fast diffusion limit may be identified with the gradual loss of MAMs due to diseases such as dry eye syndrome and eye infection (Sharma & Ruckenstein 1985). It has long been observed that the tear-film breakup time is shortened under such pathological conditions (Norn 1969; Dohlman *et al.* 1976). Our CVM prediction is consistent with these observations. Moreover, the model provides a plausible explanation for the shortened breakup time through the outward mucin diffusion from the glycocalyx.

#### 4.4. Effect of the initial viscosity profile

To explore how the initial mucin and viscosity profiles affect the nonlinear instability, we compare in figure 8 nonlinear breakup starting from the four initial profiles tested for linear stability in figure 4(a). The temporal evolution of the minimum film thickness  $h_{min}(t)$  shows that the nonlinear instability, up to film rupture, obeys the same trend discovered from linear stability analysis. That is, the profile that puts more viscous fluid near the solid wall tends to stabilize the film more and delay the film breakup (figure 4b). Along with the effect of mucin diffusion discussed above, this furnishes another example of how the simple rule established by linear analysis (§ 3.2) continues to hold into the nonlinear stages of film breakup.

Now we focus on the tanh profile only. Keeping the viscosity at the top fixed, the viscosity ratio  $\mu_r$  and the height of the mucin-rich layer  $h_m$  can be varied in concert to keep the mean viscosity of the profile constant. According to this protocol, figure 9(a) shows three initial viscosity profiles with different  $h_m$ , a smaller  $h_m$  corresponding to a thinner but more viscous mucin layer next to the wall. Figure 9(b) shows the rupture

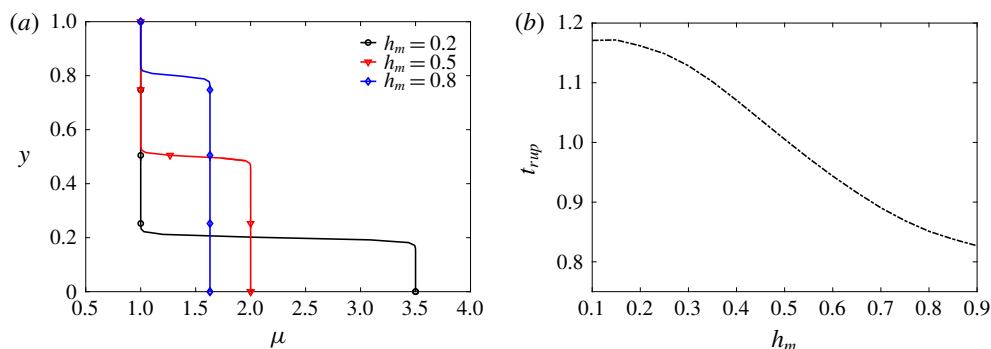


FIGURE 9. (Colour online) (a) For a fixed mean viscosity of 1.5, the initially imposed viscosity profiles for three different values of  $h_m$ . (b) Effect of  $h_m$  on the tear film rupture time  $t_{rup}$  for a healthy tear film with  $\Delta_b = 100$ .

time as a function of the initial mucin layer thickness  $h_m$ . The general trend is that the breakup time  $t_{rup}$  increases with decreasing  $h_m$ . Putting more viscous material next to the ocular surface tends to stabilize the tear film against breakup, an effect that has been confirmed repeatedly in the above. As  $h_m$  becomes very thin, however, the trend levels off. This can be rationalized by the mucin diffusion from the near-wall region toward the free surface. A smaller  $h_m$  implies a sharper mucin concentration gradient at the start, which is more quickly smeared out by diffusion after the onset of instability. Roughly speaking, the  $C$  or  $\mu$  profile will quickly relax towards that of a thicker  $h_m$  in figure 9(a). This explains how  $t_{rup}$  becomes insensitive to  $h_m$  as it gets too thin.

## 5. Comparison with TLMs

As stated in § 1, the main impetus of this study is to propose a model for tear-film breakup with a continuous mucin profile, as an alternative to the earlier models that assumed an aqueous layer atop an immiscible mucus layer. It is therefore important to compare the predictions of the new model with those of earlier models and with available experimental data. The TLM and CVM share a common limit, as noted in § 3, and figure 3(b) demonstrates that the two models yield the same linear-stability solution in that common limit. In the following, we first confirm that the two models predict the same nonlinear instability in the common limit, and then compare their predictions under conditions relevant to realistic tear films.

### 5.1. Nonlinear film rupture in the common limit

The common limit is approximated in the tanh viscosity profile by employing a sharp transition layer (with a small  $\delta_m = 10^{-4}$ ) along with slow diffusion (with a large  $\Delta_b = 100$ ). The parameters for the TLM are given in appendix A. Among these we put to zero the interfacial tension for the mucin–aqueous interface ( $C_m = 0$ ), as well as the van der Waals forces between this interface and the solid substrate and the free surface ( $\mathcal{A}_{1,2,4} = 0$ ). Figure 10 compares the CVM and TLM in the common limit for a film with  $h_m = 0.5$ , with equal initial thickness for the two layers. The two models show very close agreement in the nonlinear regime of film rupture. The nonlinear growth factor follows the linear prediction up to  $t \approx 0.5$ , after which the

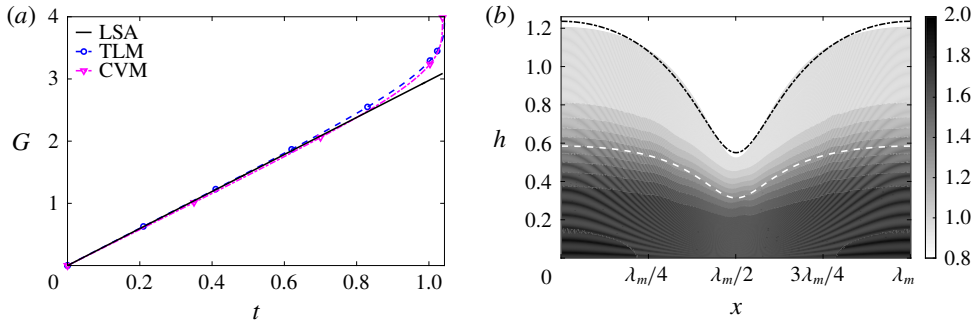


FIGURE 10. (Colour online) The common limit for the TLM and the CVM. (a) Growth of the initial perturbations with time in the TLM and CVM, in comparison with the linear growth rate (LSA). (b) The air–water and water–mucin interfaces of the TLM are superimposed on the mucin concentration field in the CVM at time  $t = 1.031$ , just before rupture.

nonlinear rate becomes increasingly greater, ending with a sharp upturn toward rupture (figure 10a). Snapshots of the interfacial profile also agree between the two models. The TLM has an air–water interface at  $h_a(x, t)$  and a mucus–aqueous layer interface at  $h_m(x, t)$ . These are overlaid on the contours of mucin concentration in the CVM (figure 10b) at  $t = 1.031$ , shortly before rupture takes place. The air–liquid interface agrees closely between the two models, and the water–mucin interface in the TLM overlaps the CVM contour  $C = 1.5$ , at the centre of the tanh profile. Thus, we have confirmed that in the limiting scenario the two models agree in both the linear and the nonlinear regimes.

### 5.2. TLM for tear film

The TLM differs from our CVM in posing an immiscible interface between the mucus and aqueous layers that possesses an interfacial tension and also interacts via van der Waals forces with the top and bottom surfaces. Bearing this in mind, we first investigate how the mucus–aqueous interfacial tension and the van der Waals attraction between the mucus–aqueous interface and the two boundaries affect the process of film breakup.

Similar studies have been performed before (Zhang *et al.* 2003a), but our case differs in allowing slip on the solid substrate in a two-layer setup. After adding the Navier slip boundary condition to the TLM of Zhang *et al.* (2003a) for Newtonian fluids, we solve these equations numerically. The predicted breakup time is depicted in figure 11 as a function of the dimensionless mucus–aqueous interfacial tension  $C_m$  for two values of the Hamaker constant  $\mathcal{A}_1$  (definitions given in appendix A). Increasing interfacial tension at the mucus–aqueous interface hinders the growth of instability. Thus, the breakup time  $t_{rup}$  increases monotonically with  $C_m$ . On the other hand, since the van der Waals attraction is the driving force for the breakup,  $t_{rup}$  decreases with increasing  $\mathcal{A}_1$ . Both trends are consistent with previous predictions using TLM in the absence of slip (Sharma & Ruckenstein 1986a,b; Zhang *et al.* 2003a).

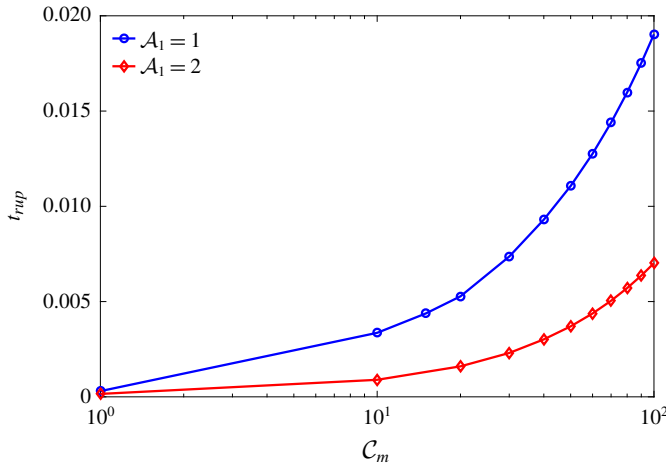


FIGURE 11. (Colour online) Effects of the interfacial tension and van der Waals attraction on the tear-film breakup time  $t_{rup}$  in the TLM. The parameter  $C_m$  is the dimensionless mucus–aqueous interfacial tension, and  $\mathcal{A}_1$  represents the aqueous–substrate interaction in the presence of the mucus layer (Zhang *et al.* 2003a). The other TLM parameters are  $h_m = 0.2$ ,  $\mu_r = 2$ ,  $\mathcal{A}_2 = \mathcal{A}_3 = \mathcal{A}_4 = 1$ ,  $\mathcal{C} = 0.1$ ,  $\mathcal{M} = 1$ ,  $Pe_s = 100$  and  $\beta = 0.1$ .

### 5.3. Comparison between CVM and TLM

A prerequisite for a meaningful comparison is to match the parameters of the two models. The complete set of parameters of the CVM are  $\mathcal{C}$ ,  $\mu_r$ ,  $h_m$ ,  $\delta_m$ ,  $\Delta_b$ ,  $Pe_s$ ,  $\beta$  and  $\mathcal{M}$ , as described in detail in § 2. On the other hand, the TLM assumes a two-layered description within the tear film and thus has a different set of governing parameters:  $\mathcal{C}$ ,  $C_m$ ,  $\mu_r$ ,  $h_m$ ,  $\mathcal{A}_1$ ,  $\mathcal{A}_2$ ,  $\mathcal{A}_3$ ,  $\mathcal{A}_4$ ,  $Pe_s$ ,  $\beta$  and  $\mathcal{M}$ , as described in detail in appendix A. Of the parameters common to both models,  $\mathcal{C}$ ,  $\mu_r$  and  $h_m$  are based on the intrinsic properties of the tear film itself and can be readily evaluated for typical tear films of the healthy eye, and matched between the two models. The other parameters are chosen on the basis of previous TLM simulations (Sharma & Ruckenstein 1986a; Zhang *et al.* 2003a). As a reference, Zhang *et al.* (2003a) adopted a power-law non-Newtonian viscosity for the mucus layer and a no-slip boundary condition on the substrate. Under these conditions, their TLM predicted a tear-film breakup time in the range of 15–50 s for healthy eyes.

We compare the two models under conditions that correspond roughly to the tear films of healthy eyes, with slip on the ocular surface (Zhang *et al.* 2003a; Braun & King-Smith 2007; Heryudono *et al.* 2007). Figure 12 plots the predicted  $t_{rup}$  for a range of  $\mathcal{C}$ , the scaled dimensionless air–tear interfacial tension. For both models,  $t_{rup}$  increases with  $\mathcal{C}$ , as one may expect. However, the predictions using the two models differ by orders of magnitude under the given set of parameters. In dimensional terms, the TLM predicts a range of  $t_{rup}$  from 0.7 s to less than 2 s for  $10^{-2} \leq \mathcal{C} \leq 1$ . Meanwhile, the CVM predicts  $t_{rup}$  ranging from 8 s to approximately 760 s over the same range of  $\mathcal{C}$ , with  $t_{rup} = 80.4$  s for the baseline value of  $\mathcal{C} = 0.1$ . It is interesting to note that our TLM predicts a much shorter  $t_{rup}$  than that of Zhang *et al.* (2003a) cited above. This is partly due to their assumption of no slip on the substrate and a power-law viscosity in the mucus layer. By imposing no-slip boundary condition in our TLM, we obtain  $t_{rup}$  between 1 and 4 s (figure 12), which is comparable to

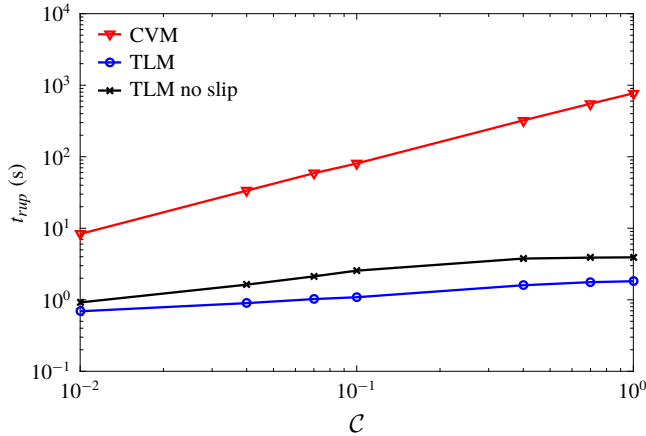


FIGURE 12. (Colour online) Comparison of the dimensional breakup time  $t_{rup}$  predicted by the TLM and CVM for a healthy tear film over a range of the air–aqueous interfacial tension  $C$ . The following parameters are common to both models:  $\mu_r = 2$ ,  $h_m = 0.2$ ,  $Pe_s = 100$ ,  $\beta = 0.1$  and  $\mathcal{M} = 1$ . In addition, we have used  $\delta_m = 0.01$  and  $\Delta_b = 100$  for the CVM, and  $C_m = 10$ ,  $\mathcal{A}_1 = \mathcal{A}_2 = \mathcal{A}_3 = \mathcal{A}_4 = 1$  for the TLM. A prediction of a no-slip TLM with  $\beta = 0$  is also plotted for comparison.

Range of $t_{rup}$ (s)	Sources
3–132	Norn (1969)
15–34	Lemp & Hamill (1973)
5–100	Vanley <i>et al.</i> (1977)
20–50	Holly & Lemp (1977)
4–214	Mengher <i>et al.</i> (1985)
> 10	Cho & Douthwaite (1992), Korb, Greiner & Herman (2001), Sullivan <i>et al.</i> (2012)

TABLE 2. Experimental data for the breakup time  $t_{rup}$  of healthy tear films.

$t_{rup} = 7.7$  s that Zhang *et al.* (2003a) predicted for a Newtonian mucus layer with no slip.

Naturally one would seek experimental data to serve as a benchmark against which to compare the predictions of the CVM and TLM. Tear-film breakup time can be measured using invasive (e.g. fluorescence imaging) as well as non-invasive (e.g. retroillumination, keratometry, corneal topography measurements) techniques (Sweeney, Millar & Raju 2013). Unfortunately, both types of measurements are affected by a variety of biological and environment factors that are difficult to control, including ambient air humidity and temperature, variations in the chemical makeup of healthy tear films, partial blinking, illumination intensity, and the concentration, pH and the type of fluorescein used. Consequently, measured  $t_{rup}$  for healthy eyes falls in a wide range, with poor reproducibility (Sweeney *et al.* 2013). Table 2 summarizes all such data as we can find in the literature.

Compared with the experimental data, the TLM prediction of  $t_{rup} = 0.7$ – $2$  s is too short, and amounts to almost instant breakup. This can be attributed to the additional van der Waals force on the thin mucus layer that is assumed in the TLM, which

hastens the rupture of the mucus–aqueous interface, and in turn making way for the breakup of the aqueous layer. Such a breakup sequence has been illustrated by Zhang *et al.* (2003a). As the dynamics of the mucus layer dominates the breakup of the whole tear film, the air–liquid interfacial tension has a relatively minor role in the TLM. Hence,  $t_{rup}$  does not vary as much with  $\mathcal{C}$  as in the CVM. In comparison, the CVM predicts  $t_{rup}$  that ranges up to hundreds of seconds, in better agreement with the measured data in table 2. This supports our initial argument that the CVM, with a suitable viscosity profile, more closely represents the true structure of the tear film than the TLM.

## 6. Conclusion

As an alternative to the prevailing TLM for the tear film, we have proposed a CVM for studying the breakup of a tear film driven by van der Waals attraction. This is motivated by experimental evidence that shows a continuous profile of mucin concentration through the thickness of the tear film, without a distinct boundary separating a mucus layer and an aqueous layer. Using linear stability analysis and nonlinear numerical simulations, we have explored how mucin and viscosity variations across the depth of the tear film affect the speed of tear-film rupture. Within the range of parameters studied, whose evaluation is based on available experimental measurements and prior modelling, the CVM predicts the following main results.

- (i) With the mean viscosity held constant, a profile that features more viscous fluids next to the solid substrate retards the growth of the interfacial instability and delays the tear-film breakup. This trend holds in the linear and nonlinear stages alike.
- (ii) Mucin diffusion affects breakup by modifying the mucin and viscosity profiles. Starting with an initial profile with higher mucin concentration near the substrate than in the upper part of the tear film, the diffusion destabilizes the film and hastens its breakup.
- (iii) The CVM predicts breakup times in better agreement than the TLM with experimental measurements for healthy tear films. This supports our intuition that the CVM better represents the structure of the tear film, and consequently its fluid dynamics.
- (iv) The lipid layer atop the tear film, treated as insoluble surfactants, has a stabilizing effect against rupture through the Marangoni stress. In contrast, the slip on the corneal epithelium destabilizes the tear film and shortens the rupture time. These effects are consistent with previous TLM predictions.

An interesting inference from the CVM prediction is that eye diseases are likely to hasten tear-film breakup, in agreement with clinical observations (Norn 1969; Dohlman *et al.* 1976; Sharma & Ruckenstein 1985). One possible mechanism is suggested by our examination of the effect of mucin diffusivity. MAMs are largely immobile, and we represent this by a low mucin diffusivity. As pathological conditions compromise the MAMs in the glycocalyx, more of the mucin can diffuse into the aqueous medium and reduce the viscosity gradient in the tear film. Our model predicts that this leads to shorter breakup times, up to a factor of about 2 (cf. figure 7). Another potential cause of faster rupture is the slip on the corneal surface, which may be aggravated by the loss of MAMs. Conceivably, both mechanisms can be tested in careful experiments that monitor the structural degradation of the corneal glycocalyx caused by eye diseases (Bron *et al.* 2015). The model predictions suggest

the interesting possibility of using the tear-film breakup as a diagnostic of the health of the glycocalyx and of impending eye infections (Yokoi *et al.* 2017). We should caution, however, that eye infection is a complex disease involving myriad factors. For example, inflammation and immune responses may change the composition and structure of the tear film as well, and such factors may complicate the linkage between tear-film breakup and eye diseases.

Finally, we should point out the shortcomings of the CVM as presented here. In building a new model that deviates from the paradigm of the layered tear-film structure, we have neglected many complicating factors that exist in the real tear film. These include, among others, evaporation, flow due to the blinking cycle, gravity-induced drainage, non-Newtonian rheology and transport of mucin due to osmosis. Many of these factors have been studied in single-layer models or TLMs (Zhang *et al.* 2003a; Jones *et al.* 2005; Siddique & Braun 2015). Moreover, there is considerable uncertainty in some of the parameter values, e.g. the mucin diffusivity and the corneal slip. For lack of experimental data, we are forced to make rough estimations. Of course, the TLM suffers from the same problem, perhaps more acutely for the greater number of parameters therein. For these reasons, we should see the present version of the CVM as a working model that attempts to better represent the structure of the tear film. By incorporating the neglected factors into the model and by evaluating the model parameters more accurately for healthy and diseased tear films, one can improve the CVM significantly in its predictive power.

### Acknowledgements

The research was supported by grants from the IC-IMPACTS Centres of Excellence (Canada) and the Department of Biotechnology (India). J.J.F. also acknowledges support by the NSERC through Discovery grant no. 05862. A.S.V. was supported by a fellowship from MHRD, Government of India, and H.N.D. acknowledges partial support from Early Career Research Award no. ECR/2015/000086.

### Appendix A. Parameters in the TLM

Consider the TLM with a mucus layer of thickness  $h_m$  below an aqueous layer, the total tear film thickness being  $h_a$ . Owing to van der Waals forces, we modify the capillary pressure inside the mucus and aqueous layers by disjoining pressures:

$$P_m = p_m + \phi_m, \quad (\text{A } 1)$$

$$P_a = p_a + \phi_a, \quad (\text{A } 2)$$

where  $p_a$ ,  $p_m$  and  $\phi_a$ ,  $\phi_m$  are the capillary and disjoining pressure terms at the two interfaces, respectively, and are expressed as

$$p_m = -Ch_{a,xx} - C_m h_{m,xx}, \quad p_a = -Ch_{a,xx}, \quad (\text{A } 3a,b)$$

$$\phi_m = \frac{\mathcal{A}_1}{h_m^3} + \frac{\mathcal{A}_2}{h_a^3}, \quad \phi_a = \frac{\mathcal{A}_3}{h_a^3} + \frac{\mathcal{A}_4}{(h_a - h_m)^3}, \quad (\text{A } 4a,b)$$

where the Hamaker constants  $\mathcal{A}_{1,2,3,4}$  are as defined in the literature (Sharma 1998; Sharma, Khanna & Reiter 1999; Zhang *et al.* 2003a; Bandyopadhyay & Sharma 2006). In our implementation, these are made dimensionless by the Hamaker constant  $\mathcal{A}$  of table 1. Of the two scaled interfacial tensions,

$$C = \frac{\epsilon^3 \sigma_a}{\mu_a V}, \quad C_m = \frac{\epsilon^3 \sigma_m}{\mu_a V}, \quad (\text{A } 5a,b)$$

$\mathcal{C}$  is for the air–aqueous interface ( $\sigma_a$  and  $\mu_a$  being the air–aqueous surface tension and the aqueous viscosity), and is identical to its CVM counterpart. Here  $\mathcal{C}_m$  is for the mucus–aqueous interface ( $\sigma_m$  being the mucus–aqueous interfacial tension), and is unique to the TLM. The surface Péclet number for the lipids and the Maragoni number are the same as in CVM:

$$Pe_s = \frac{VL}{D_s}, \quad \mathcal{M} = \frac{\epsilon \Gamma_m}{\mu_a V} \frac{\partial \Gamma}{\partial \sigma}, \quad (\text{A } 6a,b)$$

as is the Navier slip length  $\beta$ . Finally, the mucus–aqueous viscosity ratio  $\mu_r$  and the initial position of the mucus–aqueous interface  $h_m$  have counterparts in the CVM. In the above, the characteristic velocity is defined using the Hamaker constant  $\mathcal{A}$ :

$$V = \frac{\mathcal{A}}{6\pi\mu_a HL}, \quad (\text{A } 7)$$

where  $H$  and  $L$  are the characteristic thickness and horizontal length scale.

#### REFERENCES

- ALBERTSMEYER, A.-C., KAKKASSERY, V., SPURR-MICHAUD, S., BEEKS, O. & GIPSON, I. K. 2010 Effect of pro-inflammatory mediators on membrane-associated mucins expressed by human ocular surface epithelial cells. *Exp. Eye Res.* **90** (3), 444–451.
- BANDYOPADHYAY, D. & SHARMA, A. 2006 Nonlinear instabilities and pathways of rupture in thin liquid bilayers. *J. Chem. Phys.* **125**, 054711.
- BERGER, R. & CORRSIN, S. 1974 A surface tension gradient mechanism for driving the pre-corneal tear film after a blink. *J. Biomech.* **7**, 225–238.
- BRAUN, R. & KING-SMITH, P. E. 2007 Model problems for the tear film in a blink cycle: single equation models. *J. Fluid Mech.* **586**, 465–490.
- BRAUN, R. J. 2012 Dynamics of tear films. *Annu. Rev. Fluid Mech.* **44**, 267–297.
- BRAUN, R. J., DRISCOLL, T. A., BEGLEY, C. G., KING-SMITH, P. E. & SIDDIQUE, J. I. 2018 On tear film breakup (TBU): dynamics and imaging. *Math. Med. Biol.* **35**, 145–180.
- BRAUN, R. J., USHA, R., MCFADDEN, G. B., DRISCOLL, T. A., COOK, L. P. & KING-SMITH, P. E. 2012 Thin film dynamics on a prolate spheroid with application to the cornea. *J. Engng Maths* **73**, 121–138.
- BRON, A. J., ARGÜESO, P., IRKEC, M. & BRIGHT, F. V. 2015 Clinical staining of the ocular surface: mechanisms and interpretations. *Prog. Retin. Eye Res.* **44**, 36–61.
- BRON, A. J., TIFFANY, J. M., GOUVEIA, S. M., YOKOI, N. & VOON, L. W. 2004 Functional aspects of the tear film lipid layer. *Exp. Eye Res.* **78**, 347–360.
- BRUNA, M. & BREWARD, C. J. W. 2014 The influence of non-polar lipids on tear film dynamics. *J. Fluid Mech.* **746**, 565–605.
- BURELBACH, J. P., BANKOFF, S. G. & DAVIS, S. H. 1988 Nonlinear stability of evaporating/condensing liquid films. *J. Fluid Mech.* **195**, 464–494.
- CELLI, J., GREGOR, B., TURNER, B., AFDHAL, N. H., BANSIL, R. & ERRAMILI, S. 2005 Viscoelastic properties and dynamics of porcine gastric mucin. *Biomacromolecules* **6**, 1329–1333.
- CHEN, H. B., YAMABAYASHI, S., TANAKA, Y., OHNO, S. & TSUKAHARA, S. 1997 Structure and composition of rat precorneal tear film: a study by an in vitro cryofixation. *Invest. Ophthalmol. Vis. Sci.* **38**, 381–387.
- CHO, P. & DOUTHWAITE, W. 1992 Tear breakup time and the effect of lifting the eyelid during its measurement. *Clin. Exp. Optom.* **75**, 231–235.

- CRAIG, J. & TOMLINSON, A. 1997 Importance of the tear film lipid layer in human tear film stability and evaporation. *Optom. Vis. Sci.* **33**, 8–13.
- CRASTER, R. V. & MATAR, O. K. 2009 Dynamics and stability of thin liquid films. *Rev. Mod. Phys.* **81**, 1131–1198.
- DE WIT, A., GALLEZ, D. & CHRISTOV, C. I. 1994 Nonlinear evolution equations for thin liquid films with insoluble surfactants. *Phys. Fluids* **6**, 3256–3266.
- DENG, Q., BRAUN, R. J. & DRISCOLL, T. A. 2014 Heat transfer and tear film dynamics over multiple blink cycles. *Phys. Fluids* **26**, 071901.
- DOHLMAN, C. H., FRIEND, J., KALEVAR, V., YAGODA, D. & BALAZS, E. 1976 The glycoprotein (mucus) content of tears from normals and dry eye patients. *Exp. Eye Res.* **22**, 359–365.
- ERN, P., CHARRU, F. & LUCHINI, P. 2003 Stability analysis of a shear flow with strongly stratified viscosity. *J. Fluid Mech.* **496**, 295–312.
- GHOSH, S., USHA, R. & SAHU, K. C. 2014 Linear stability analysis of miscible two-fluid flow in a channel with velocity slip at the walls. *Phys. Fluids* **26**, 014107.
- GIPSON, I. K. 2004 Distribution of mucins at the ocular surface. *Exp. Eye Res.* **78**, 379–388.
- GOVINDARAJAN, B. & GIPSON, I. K. 2010 Membrane-tethered mucins have multiple functions on the ocular surface. *Exp. Eye Res.* **90**, 655–663.
- GRIBBON, P. & HARDINGHAM, T. E. 1998 Macromolecular diffusion of biological polymers measured by confocal fluorescence recovery after photobleaching. *Biophys. J.* **75**, 1032–1039.
- HERYUDONO, A., BRAUN, R. J., DRISCOLL, T. A., MAKI, K. L., COOK, L. P. & KING-SMITH, P. E. 2007 Single-equation models for the tear film in a blink cycle: realistic lid motion. *Math. Med. Biol.* **24**, 347–377.
- HODGES, R. R. & DARTT, D. A. 2013 Tear film mucins: front line defenders of the ocular surface; comparison with airway and gastrointestinal tract mucins. *Exp. Eye Res.* **117**, 62–78.
- HOLLY, F. J. & LEMP, M. A. 1977 Tear physiology and dry eyes. *Surv. Ophthalmol.* **22**, 69–87.
- INATOMI, T., SPURR-MICHAUD, S., TISDLE, A. S., ZHAN, Q., FELDMAN, S. T. & GIPSON, I. K. 1996 Expression of secretory mucin genes by human conjunctival epithelia. *Invest. Ophthalmol. Vis. Sci.* **37**, 1684–1692.
- JONES, M. B., PLEASE, C. P., MCELWAIN, D. L., FULFORD, G. R., ROBERTS, A. P. & COLLINS, M. J. 2005 Dynamics of tear film deposition and draining. *Math. Med. Biol.* **22**, 265–288.
- JOSSIC, L., LEFEVRE, P., LOUBENS, C., MAGNIN, A. & CORRE, C. 2009 The fluid mechanics of shear-thinning tear substitutes. *J. Non-Newtonian Fluid Mech.* **161**, 1–9.
- KING-SMITH, P. E., BEGLEY, C. G. & BRAUN, R. J. 2018 Mechanisms, imaging and structure of tear film breakup. *Ocul. Surf.* **16**, 4–30.
- KORB, D. R., GREINER, J. V. & HERMAN, J. 2001 Comparison of fluorescein break-up time measurement reproducibility using standard fluorescein strips versus the dry eye test (DET) method. *Cornea* **20**, 811–815.
- LEMP, M. A. & HAMILL, J. R. 1973 Factors affecting tear film breakup in normal eyes. *Arch. Ophthalmol.* **89**, 103–105.
- LIU, H., BEGLEY, C., CHEN, M., BRADLEY, A., BONANNO, J., MCNAMARA, N. A., NELSON, J. D. & SIMPSON, T. 2009 A link between tear instability and hyperosmolarity in dry eye. *Invest. Ophthalmol. Vis. Sci.* **50**, 3671–3679.
- MANTELLI, F. & ARGUESO, P. 2008 Functions of ocular surface mucins in health and disease. *Curr. Opin. Allergy Clin. Immunol.* **8**, 477–483.
- MATAR, O. 2002 Nonlinear evolution of thin free viscous films in the presence of soluble surfactant. *Phys. Fluids* **14**, 4216–4234.
- MCCULLEY, J. P. & SHINE, W. 1997 A compositional based model for the tear film lipid layer. *Trans. Am. Ophthalmol. Soc.* **95**, 79–93.
- MENGER, L. S., BRON, A. J., TONGE, S. R. & GILBERT, D. J. 1985 A non-invasive instrument for clinical assessment of the precorneal tear film stability. *Curr. Eye Res.* **4**, 1–7.
- NAGYOVÁ, B. & TIFFANY, J. M. 1999 Components responsible for the surface tension of human tears. *Curr. Eye Res.* **19**, 4–11.

- NORN, M. S. 1969 Desiccation of the precorneal film. Part I. Corneal wetting-time. *Acta Ophthalmol.* **47**, 865–880.
- ORON, A., DAVIS, S. H. & BANKOFF, S. G. 1997 Long-scale evolution of thin liquid films. *Rev. Mod. Phys.* **69**, 931–980.
- PENG, C. C., CERRETANI, C., BRAUN, R. J. & RADKE, C. J. 2014 Evaporation-driven instability of the precorneal tear film. *Adv. Colloid Interface Sci.* **206**, 250–264.
- POTOTSKY, A., BESTEHORN, M., MERKT, D. & THIELE, U. 2004 Alternative pathways of dewetting for a thin liquid two-layer film. *Phys. Rev. E* **70** (2), 025201.
- PRYDAL, J. I. & CAMPBELL, F. W. 1992 Study of precorneal tear film thickness and structure by interferometry and confocal microscopy. *Invest. Ophthalmol. Vis. Sci.* **33**, 1996–2005.
- RUCKENSTEIN, E. & JAIN, R. K. 1974 Spontaneous rupture of thin liquid films. *J. Chem. Soc., Faraday Trans. 2* **70**, 132–147.
- SELINGER, D. S., SELINGER, R. C. & REED, W. P. 1979 Resistance to infection of the external eye: the role of tears. *Surv. Ophthalmol.* **24**, 33–38.
- SHARMA, A. 1998 Acid–base interactions in the cornea-tear film system: surface chemistry of corneal wetting, cleaning, lubrication, hydration and defense. *J. Dispersion Sci. Technol.* **19**, 1031–1068.
- SHARMA, A., KHANNA, R. & REITER, G. 1999 A thin film analog of the corneal mucus layer of the tear film: an enigmatic long range non-classical DLVO interaction in the breakup of thin polymer films. *Colloids Surf. B* **14**, 223–235.
- SHARMA, A. & RUCKENSTEIN, E. 1985 Mechanism of tear film rupture and formation of dry spots on cornea. *J. Colloid Interface Sci.* **106**, 12–27.
- SHARMA, A. & RUCKENSTEIN, E. 1986a An analytical nonlinear theory of thin film rupture and its application to wetting films. *J. Colloid Interface Sci.* **113**, 456–479.
- SHARMA, A. & RUCKENSTEIN, E. 1986b The role of lipid abnormalities, aqueous and mucus deficiencies in the tear film breakup, and implications for tear substitutes and contact lens tolerance. *J. Colloid Interface Sci.* **111**, 8–34.
- SIDDIQUE, J. I. & BRAUN, R. J. 2015 Tear film dynamics with evaporation, osmolarity and surfactant transport. *Appl. Math. Model.* **39**, 255–269.
- STEVENSON, W., CHAUHAN, S. K. & DANA, R. 2012 Dry eye disease: an immune-mediated ocular surface disorder. *Arch. Ophthalmol.* **130**, 90–100.
- SULLIVAN, B. D., CREWS, L. A., SONMEZ, B., DE LA PAZ, M. F., COMERT, E., CHAROENROOK, V., DE ARAUJO, A. L., PEPOSE, J. S., BERG, M. S., KOSHELEFF, V. P. & LEMP, M. A. 2012 Clinical utility of objective tests for dry eye disease: variability over time and implications for clinical trials and disease management. *Cornea* **31**, 1000–1008.
- SWEENEY, D. F., MILLAR, T. J. & RAJU, S. R. 2013 Tear film stability: a review. *Exp. Eye Res.* **117**, 28–38.
- TIFFANY, J. M. 1991 The viscosity of human tears. *Intl Ophthalmol.* **15**, 371–376.
- USHA, R., TAMMISOLA, O. & GOVINDARAJAN, R. 2013 Linear stability of miscible two-fluid flow down an incline. *Phys. Fluids* **25**, 104102.
- VANLEY, G. T., IRVING, B. A., LEOPOLD, H. & GREGG, T. H. 1977 Interpretation of tear film break-up. *Arch. Ophthalmol.* **95**, 207–209.
- WILLIAM, M. B. & DAVIS, S. H. 1982 Nonlinear theory of film rupture. *J. Colloid Interface Sci.* **90**, 220–228.
- WINTER, K. N., ANDERSON, D. M. & BRAUN, R. J. 2010 A model for wetting and evaporation of a post-blink precorneal tear film. *Math. Med. Biol.* **27**, 211.
- YAÑEZ-SOTO, B., MANNIS, M. J., SCHWAB, I. R., LI, J. Y., LEONARD, B. C., ABBOTT, N. L. & MURPHY, C. J. 2014 Interfacial phenomena and the ocular surface. *Ocul. Surf.* **12**, 178–201.
- YOKOI, N., GEORGIEV, G., KATO, H., KOMURO, A., SONOMURA, Y., SOTOZONO, C., TSUBOTA, K. & KINOSHITA, S. 2017 Classification of fluorescein breakup patterns: a novel method of differential diagnosis for dry eye. *Am. J. Ophthalmol.* **180**, 72–85.
- ZHANG, Y. L., CRASTER, R. V. & MATAR, O. K. 2003a Analysis of tear film rupture: effect of non-Newtonian rheology. *J. Colloid Interface Sci.* **262**, 130–148.

- ZHANG, Y. L., CRASTER, R. V. & MATAR, O. K. 2003*b* Surfactant driven flows overlying a hydrophobic epithelium: film rupture in the presence of slip. *J. Colloid Interface Sci.* **264**, 160–175.
- ZHANG, Y. L., CRASTER, R. V. & MATAR, O. K. 2004 Rupture analysis of the corneal mucus layer of the tear film. *Mol. Simul.* **30**, 167–172.
- ZHONG, L., KETELAAR, C. F., BRAUN, R. J., BEGLEY, C. G. & KING-SMITH, P. E. 2018 Mathematical modelling of glob-driven tear film breakup. *Math. Med. Biol.* doi:[10.1093/imammb/dqx021](https://doi.org/10.1093/imammb/dqx021).